Accepted Manuscript

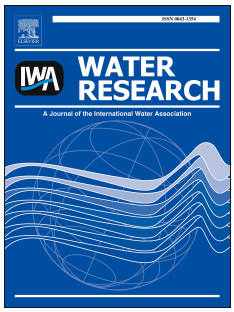

Interaction between bacterial cell membranes and nano-TiO_2 revealed by two-dimensional FTIR correlation spectroscopy using bacterial ghost as a model cell envelope

Guocheng Huang, Tsz Wai Ng, Taicheng An, Guiying Li, Bo Wang, Dan Wu, Ho Yin Yip, Huijun Zhao, Po Keung Wong

PII: S0043-1354(17)30282-8

DOI: 10.1016/j.watres.2017.04.023

Reference: WR 12820

To appear in: *Water Research*

Received Date: 20 January 2017

Revised Date: 4 April 2017

Accepted Date: 8 April 2017

Please cite this article as: Huang, G., Ng, T.W., An, T., Li, G., Wang, B., Wu, D., Yip, H.Y., Zhao, H., Wong, P.K., Interaction between bacterial cell membranes and nano-TiO_2 revealed by two-dimensional FTIR correlation spectroscopy using bacterial ghost as a model cell envelope, *Water Research* (2017), doi: 10.1016/j.watres.2017.04.023.

Graphic Abstract

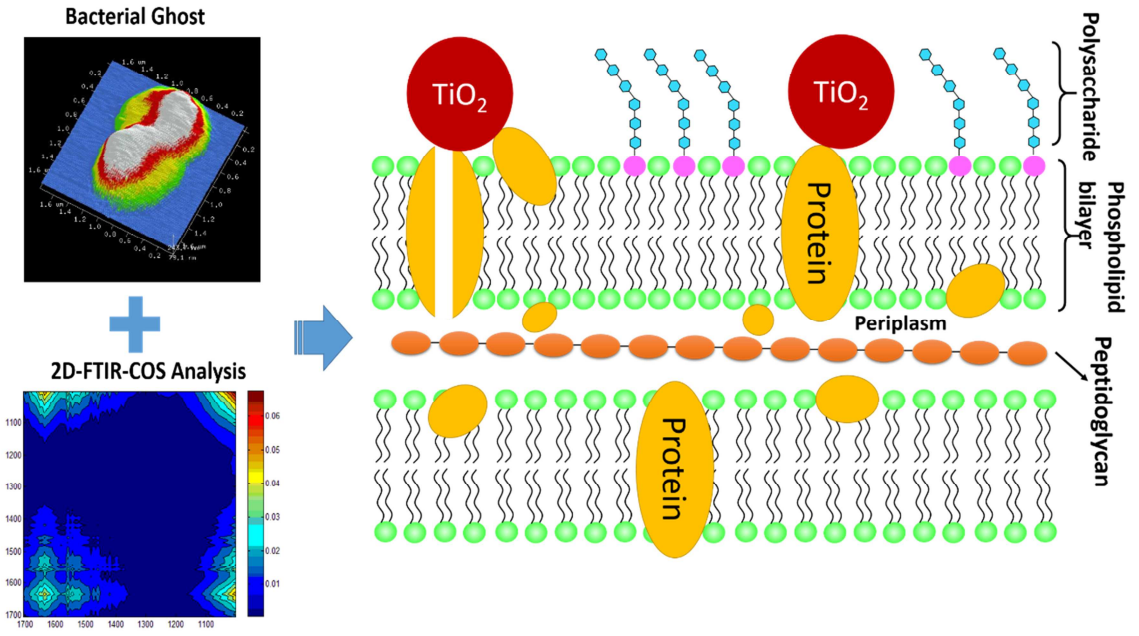

Interaction between bacterial cell membranes and nano-TiO_2 revealed by two-dimensional FTIR correlation spectroscopy using bacterial ghost as a model cell envelope

Guocheng Huang [a], Tsz Wai Ng [a], Taicheng An [b,*], Guiying Li [b], Bo Wang [a], Dan Wu [a], Ho Yin Yip [a], Huijun Zhao [c], and Po Keung Wong [a,*]

[a] School of Life Sciences, The Chinese University of Hong Kong, Shatin, NT, Hong Kong SAR, China

[b] Institute of Environmental Health and Pollution Control, School of Environmental Science and Engineering, Guangdong University of Technology, Guangzhou 510006, China

[c] Centre for Clean Environment and Energy, Griffith Scholl of Environment, Griffith University, Queensland 4222, Australia

*__Corresponding authors:__ Tel: +86 20 2388 3536, Fax: +86 20 8529 1501, E-mail: antc99@gdut.edu.cn (T.C. An); Tel: +852 3943 6383, Fax: +852 2603 5767, E-mail: pkwong@cuhk.edu.hk (P.K. Wong).

Abstract

The interaction between microorganisms and nanoparticles is a crucial step towards understanding the subsequent biological effect. In this study, the interaction between TiO_2 nanoparticles and bacterial cell membrane was investigated by Two-dimensional Correlation Fourier Transformation Infrared spectroscopy (2D-FTIR-COS) using bacterial ghosts (BGs), which are non-living bacterial cell envelopes devoid of cytoplasm. The synchronous map of 2D-FTIR-COS results indicated that the functionalities in proteins of BGs preferentially interacted with TiO_2 nanoparticles; whereas the interaction of TiO_2 nanoparticles with characteristic functionality in polysaccharides (C–OH) and phospholipids (P=O) were very weak or insensitive. This conclusion was further corroborated by settling of TiO_2 nanoparticles in the presence of pure protein, polysaccharide and phospholipid represented by bovine serum albumin (BSA), alginate and phosphatidylethanolamine (PE). Additionally, the asynchronous map of 2D-FTIR-COS indicated a sequential order of functionalities bonded to TiO_2 nanoparticles with the order of: COO^- > aromatic C=C stretching > N-H, amide II > C=O, ketone. These findings contribute to deeper understanding of the interaction between TiO_2 nanoparticles and bacterial cell membrane in aquatic systems.

Keywords: Titanium dioxide nanoparticles; Bacterial ghosts; Two-dimensional FTIR correlation; Nanoparticle-cell membrane interaction

1. Introduction

Titanium dioxides (TiO_2) nanoparticles is one of the most widely used nanomaterials, with applications as cosmetics (Auffan *et al.*, 2010), sunscreens (Nohynek *et al.*, 2007), food additives (Weir *et al.*, 2012) and photocatalysts (Hoffmann *et al.*, 1995). The annual production of TiO_2 nanoparticles is rapidly increasing and estimated to reach 2.5 million metric tons by 2025 (Menard *et al.*, 2011). Due to the increased production and application of synthetic TiO_2 nanoparticles, their release into the environment is inevitable. However, information regarding the TiO_2 nanoparticles toxicity, transport and fate in both natural and engineered systems is still scarce. Based on the existing studies, it is proposed that the interaction between nanoparticles and the membranes of microorganisms can be a critical initial process that precedes the toxicity pathways as well as influences the environmental fate of nanoparticles (Chen and Bothun, 2014).

To date, most related investigation on the interaction between cells and nanoparticles were mainly focused on how water chemistry, such as pH and ionic strength, affect the interaction between cells and nanoparticles (French *et al.*, 2009; Ma *et al.*, 2015). For example, solution pH determines the surface charges (i.e. zeta potentials) of both cells and nanoparticles, and thus influences the electrostatic interaction profile between the two objects. It was observed in many studies that low pH enhanced this interaction due to the nanoparticles being more positively charged while cells remaining negatively charged (Khan *et al.*, 2011; Schwegmann *et al.*, 2013). Salt ions can compress the electro-double layer of nanoparticles and cells, thereby reducing or eliminating the electro-double layer interaction. As a consequence, the commonly attractive van der Waals force becomes dominated and results in enhancement of cell surface and nanoparticle interaction under high ionic strength in water (Mukherjee and Weaver, 2010; Li *et al.*, 2011; Shih *et al.*, 2012). These

results could be well described by the Derjaguin-Landau-Verwey-Overbeek (DLVO) theory due to the fact that the sizes of both microorganism cells and nanoparticles aggregates are within the scale of colloids. More recently, more comprehensive studies on the interaction between cell surface and nanoparticle in the presence of natural organic matters (NOM) have been carried out to mimic natural water environment (Lin *et al.*, 2012). It was pointed out that the both bulk and nanoparticle-bound NOM can inhibit the interaction between cells and nanoparticles due to the delivery of negative charge to the surface of TiO_2 nanoparticles by NOM.

Approaches to probe the nanoparticle-membrane interaction are quite diverse, including by atomic force microscopy (AFM) (Leroueil *et al.*, 2007; Roiter *et al.*, 2008), optical tweezers (Rusciano *et al.*, 2009), and quartz crystal microbalance with dissipation monitoring (QCM-D) (Keller and Kasemo, 1998; Zhang and Yang, 2011). QCM-D is the most extensively used tool for nanoparticle-membrane interaction due to its ability to in situ detection of nanoparticles adsorption on model cell membranes at a sensitivity level as low as tens of nanograms (Chen and Bothun, 2014). However, these techniques cannot distinguish which constituents or functionality of cell membrane correspond to the interaction when a membrane with multiple constituents is applied. Therefore, the binding affinities of cell surface constituents or functional groups to nanoparticles are unexplored.

Fourier transform-infrared (FTIR) spectroscopy is a versatile technique that offers a comprehensive insight into the molecular structure of principle constituents in bacterial cell membranes, such as protein, polysaccharide and lipid (Mecozzi *et al.*, 2009). Two-dimensional correlation spectra (2D-COS), developed by Noda (1993), can be applied to resolve the overlapped peaks by distributing the spectral intensity trends along a second dimension with the data set

collected as a function of a perturbation (e.g. time, temperature, concentration, etc.) (Noda, 1993; Dluhy *et al.*, 2006). More importantly, it can also provide the information about the relative direction and sequential orders of structural variations in response to the perturbation. Thus, 2D-COS has been successfully applied to explore the interaction processes of NOM and TiO_2 nanoparticles (Chen *et al.*, 2014). To the best of our knowledge, there is no literature reporting the application of 2D-FTIR-COS in the investigation on the interaction between nanoparticles and biological relevant components.

So far, the molecular mechanisms of the interaction between the NPs and bacterial cell membrane remain unclear, particularly, information on adsorption affinities of individual molecular constituents and functional groups is lacking. One of the major challenges is that cell membrane is dynamic and heterogeneous comprising multiple components such as phospholipid, protein, and polysaccharide (Chen and Bothun, 2014) that can lead to a more elaborate analysis of the mechanisms involved. Another challenge is that live cells undergoing metabolic process would secrete soluble microbial product (SMP) into the reaction solution and undoubtedly affect the interaction profile between cell surface and nanoparticles (Ni *et al.*, 2011). A strategy to carry out nanoparticle-membrane interaction studies is to employ model membrane systems based on the phospholipid bilayer backbone of the cell membrane such as lipid vesicles (Hou *et al.*, 2012; Lesniak *et al.*, 2013; Chen and Bothun, 2014). Such systems can be further elaborated on by introducing other relevant components (i.e. protein and polysaccharides) that will make them more resemble the structure of cell membrane. Nevertheless, the synthesis of multi-components membrane architectures requires complex procedures and studies employing model membranes with embedded constituents such as protein and polysaccharide is still lacking to completely

explore the interaction mechanism.

Bacterial ghosts (BGs) have recently emerged as novel vaccine candidates owing to their properties of being non-living bacterial cell membrane structure (cell envelopes) devoid of cytoplasmic constituents, and maintaining the full cellular morphology and surface constituents of their living counterparts (Jalava *et al.*, 2002; Kudela *et al.*, 2010). Moreover, the BGs can be easily produced by genetic methods or chemical methods (Mayr *et al.*, 2005; Amara *et al.*, 2013b). Therefore, it will be advantageous to employ BGs to study the interaction mechanisms of nanoparticles and cell membrane.

The purpose of this study, therefore, is to investigate the interaction between TiO_2 nanoparticles and cell membrane, by 2D-FTIR-COS technique, with BG as a model system. The settling experiments of standard protein, polysaccharide and phospholipid with TiO_2 were carried out to further verify and support the results.

2. Material and methods

2.1 Cell cultures and TiO_2 nanoparticles.

Escherichia coli (*E. coli*) K-12 was used as model bacterium in this study. The bacterial cells were cultured in 50 mL Nutrient Broth 'E' (Lancashire, UK) with agitation at 200 rpm for 16 h. The cultures were then washed twice with sterile saline solution (0.9% NaCl) and resuspended in 50 mL sterilized saline solution with a cell density of ~2×10^9 colony forming unit per milliliter (cfu/mL). Degussa TiO_2 (P25, German) was used as a model TiO_2 nanoparticles in this study. The crystalline structures of the TiO_2 nanoparticles were identified through X-ray diffraction (XRD) analysis (Fig.

S1). Its crystal structure consists of 80% anatase and 20% rutile, with an average primary size of 20-30 nm as revealed by transmission electron microscopic (TEM) analysis (Fig. S2), which were consistent with the description of manufacturer and published literatures (Chowdhury *et al*., 2011; Tong *et al*., 2013a). A stock solution containing 10 g/L P25 solutions was used to prepare different concentrations of TiO_2 solutions.

2.2 BGs preparation and characterizations.

The BGs were prepared according to a chemical method named "sponge-like" protocol (Amara *et al.*, 2013a; Amara *et al.*, 2013b). This method based on using active chemical reagents in concentration between Minimum Inhibition Concentration (MIC) and Maximum Growth Concentration (MGC) for bacteria. The MIC and MGC of were determined according to a previous report (Andrews, 2001), and shown in Table S1. Four chemical reagents were used in this protocol and their applied concentrations are determined as 4 mg/mL for SDS, 0.02 M for NaOH, 1.05 μg/mL for $CaCO_3$ and 64 mM for H_2O_2. In brief, 50 mL of washed cells were incubated with SDS, $CaCO_3$ and NaOH for 1 h to produce micropores on the surface of bacteria cells. Then the mixtures were centrifuged at 4,000 rpm (Hermle Z323, Germany) for 10 min to evacuate the cytoplasmic constituent. The cell pellets were then washed with sterilized saline solution and resuspended in H_2O_2 solution for 30 min to guarantee the degradation of the residual DNA. Finally, the cells were collected by centrifugation at 4,000 rpm and resuspended in 60% ethanol to remove any soluble organic residual. Then BGs were harvested by centrifugation at 4,000 rpm and resuspended in 50 mL ultrapure water.

Light microscopy, scanning electronic microscope (SEM) and atomic force microscope (AFM) were used to observe the BGs as well as the normal bacterial cells. Detailed descriptions of these

129 works can be found in the supporting information. The DNA in the BGs and normal bacterial cells
130 were, respectively, extracted using a Takara MiniBEST DNA Extraction Kit. DNA agarose gel
131 electrophoresis (AGE) was also performed with 0.6% agarose gel at 80 V for 45 min in TAE buffer
132 (40 mM Tris-acetate/1 mM EDTA, pH=8) to determine the existence of any residual DNA in the
133 BGs. The concentrations of extracted DNA were determined via a Nanodrop spectrophotometry
134 (Model 2000C, Thermo Scientific, Waltham, MA, USA).

135

136 **2.3 Interaction of BGs with TiO_2 nanoparticles.**

137 The BGs suspension was diluted to a concentration equivalent to ~2×10^8 cfu/mL in all the
138 experiments unless otherwise stated. A series of BGs suspensions containing different
139 concentrations of TiO_2 nanoparticles ranging from 0 - 200 mg/L were prepared and the final
140 solution pH was adjusted to circumneutral condition (~ 6.8) using 0.01 M HCl and 0.01 M NaOH,
141 which is close to the isoelectric point (IEP) of the TiO_2 nanoparticles (Huang *et al.,* 2015). This pH
142 condition can minimize the long-range electrostatic interaction (non-molecular interaction) and was
143 environmental relevant (Parikh and Chorover, 2006). Then the suspensions were under vigorous
144 agitation of 200 rpm for 8 h at 25 ^{o}C under dark in an incubator. Finally, 20 mL of each suspensions
145 was sampled and freeze-dried for the FTIR measurement.

146

147 **2.4 Spectroscopic parameters.**

148 An FTS-4000 Varian Excalibur series FT-IR spectrometer with attenuated total reflection (ATR)
149 (Varian, Palo Alto, CA) was used to collect the infrared spectra. A mixture of the freeze-dried
150 samples and 100 mg of potassium bromide (KBr, IR grade) were ground, homogenized and pressed.

The band from 4000 to 400 cm^{-1} were collected with an interval of 2 cm^{-1}, and the ordinate was express as absorbance. Each spectrum was an average of 256 scans with automatic baseline correction. The obtained spectra were then smoothed using OMNIC 8.0 software for the subsequent analysis. The spectra of amide I region (1700-1600 cm^{-1}) were further analyzed to extract information regarding changes of the protein secondary structures by deconvolved spectra. A detailed description of the procedure can be found in the supporting information.

To assess the secretion of soluble microbial product (SMP) from normal cells of *E. coli* K-12, which may influence the interaction profile between TiO_2 nanoparticles and cell membranes, suspensions with 50 mL 2×10^8 cfu/mL normal *E. coli* K-12 cells were prepared under dark in the absence and presence of 100 mg/L TiO_2 P25 and shaken at 25 ^oC. Three mL suspension was sampled and filtered through a 0.22 μm nylon membrane to remove cells or/and TiO_2 nanoparticles at different time intervals. Then the filtrate was analyzed with a fluorescence spectrophotometer (F-7000, Hitachi, Japan) in excitation-emission-matrix (EEM) mode. Fluorescence EEM is a powerful tool to characterize SMP based on well-established principles (Hudson *et al.*, 2007). For comparison, the fluorescence EEM of the bulk solution of BGs in the absence and presence of TiO_2 nanoparticles were also monitored.

2.5 2D-FTIR-COS analysis.

In this study, the TiO_2 nanoparticles concentration was applied as an external perturbation, and a set of concentration-dependent FT-IR spectra was obtained. Before conducting 2D-FTIR-COS, each FTIR spectrum was baseline-corrected and smoothed using Savitzky-Golay method (Wang *et al.*, 2012; Chen *et al.*, 2014). The practical computation of 2D-FTIR-COS was performed using

Matlab R2010a (Mathworks Inc., USA) (Noda, 1993; Chen *et al.*, 2015). The synchronous correlation intensity can be constructed using the following equation:

$$\phi(\upsilon_1, \upsilon_2) = \frac{1}{m-1}\sum_{j=1}^{m} I_j(\upsilon_1) I_j(\upsilon_2) \quad (1)$$

Asynchronous correlation can be calculated by:

$$\varphi(\upsilon_1, \upsilon_2) = \frac{1}{m-1}\sum_{j=1}^{m} I_j(\upsilon_1) \sum_{j=1}^{m} N_{jk} I_j(\upsilon_2) \quad (2)$$

Where m is the total number of the collected spectra, $I_j(\upsilon)$ represents the intensity of the jth spectrum collected at a specific band or wavenumber of υ (denoting with a subscript of "1" or "2"). The term N_{jk} corresponds to the jth column and the kth row element of the discrete Hilbert-Noda transform matrix, which is defined as:

$$N_{jk} = \begin{cases} 0 & \text{if } j = k \\ \dfrac{1}{\pi(k-j)} & \text{otherwise} \end{cases} \quad (3)$$

The sign of the synchronous peaks $\phi(\upsilon_1, \upsilon_2)$ reflects simultaneous changes in intensities measured at υ_1 and υ_2 in response to perturbation (Dluhy *et al.*, 2006). A positive sign, $\phi(\upsilon_1, \upsilon_2) > 0$, indicates the intensities change in the same direction (either increase or decrease simultaneously), while the trend is reversed for $\phi(\upsilon_1, \upsilon_2) < 0$. The sign of the asynchronous peak

193 $\varphi(\upsilon_1, \upsilon_2)$ reflects the sequential order of the intensity change measured at υ_1 and υ_2 in response
194 to perturbation. If $\phi(\upsilon_1, \upsilon_2)$ and $\varphi(\upsilon_1, \upsilon_2)$ have the same sign, the intensity change at υ_1 occurs
195 predominantly before υ_2 while the rule is reversed if $\phi(\upsilon_1, \upsilon_2)$ and $\varphi(\upsilon_1, \upsilon_2)$ have the opposite
196 sign.

197

198 **2.6 TiO_2 precipitation with standard protein, polysaccharide and phospholipid.**

199 To further verify the role of the key biomolecular constituents in cell membrane in the
200 interaction with TiO_2 nanoparticles, a series of settling experiments were performed according to
201 previous studies (Lin *et al.*, 2012; Ma *et al.*, 2015). Bovine serum albumin (BSA), sodium alginate
202 and phosphatidylethanolamine (PE) were used as standard biomolecular constituents to represent
203 protein, polysaccharide and phospholipid, respectively. The mixed suspensions of 100 mg/L TiO_2
204 nanoparticles and biomolecular constituents with concentrations ranging from 0 to 200 mg/L were
205 prepared (pH=6.8) and subjected to settling experiments for 11 h, and their individual suspensions
206 were also conducted as control. At different settling time, 1 mL aliquot of the mixed and individual
207 suspensions were taken from the top of the suspension and immediately transferred into cuvettes to
208 measure absorbance at 660 nm (A_{660}). The settling curves were plotted using the ratio of absorbance
209 at a given time point (A_t) to the initial absorbance (A_0) as coordinate and time as abscissa.

210

211 ## 3. Results

212 **3.1 BGs as model cell envelope.**

213 To examine whether normal cells will secrete any SMP into the bulk solution, fluorescence
214 EEM was applied to show the spectra of SMP secreted by normal cells of *E. coli* K-12 cells in the

absence and presence of TiO_2 nanoparticles (Fig. 1). The peaks at Ex/Em of 230/340 nm (peak T1) and 280/340 nm (peak T2) are reported to be associated with the tryptophan-like protein, (Hudson *et al.*, 2007) which is a common fluorescent SMP secreted by bacterial cells. For *E. coli* cells under dark (Fig. 1a), the peak intensities increased along with time (Fig. S3a), suggesting that SMP was secreted into the bulk solution. With the addition of TiO_2 nanoparticles, the peak intensities still exhibited an increasing trend (Fig. 1b) along with time, while lower than those of sole *E. coli* cells at each time point (Fig. S3a). This difference was due to the released SMP adsorbing on the TiO_2 and thus led to a decrease of SMP concentration in the bulk solution. Therefore, the investigation of interaction between TiO_2 nanoparticles and cell membrane will certainly be affected by the presence of these release metabolic products. For example, it has been well-recognized that protein absorbed on nanoparticles surface to form nanoparticle-protein 'corona' (Mahon *et al.*, 2012; Lesniak *et al.*, 2013; Saptarshi *et al.*, 2013), which would ultimately determine the interaction profile of nanoparticles with the biological membrane systems, rather than the pristine surface of the unmodified nanoparticles. For example, a previous study found that protein adsorption onto nanoparticles reduced their ability to adhere to cell surface (Lesniak *et al.*, 2013). Therefore, employing model cell envelopes such as BGs, which lack metabolic activities, are of important merit to reveal an unbiased nanoparticle-membrane interaction mechanism.

To avoid the interference of SMP, BGs as model cell envelope was applied as model cell membrane in this study. Fig. 2 compares the SEM and AFM images of normal bacterial cell and BGs. The SEM and AFM images proved that the BGs were in good conditions and still maintained the 3D structure with micropores on the surface which were consistent with previous studies on the morphology of BGs (Amara *et al.*, 2013b). Besides, the crystal violet stained BGs could be

observed by light microscopy (Fig. S4), which was indicative of stable cell envelopes structure. Furthermore, the agarose gel electrophoresis results shown that no observable band on the lane of the BGs compared with the normal bacterial cells of *E. coli* K-12 (Fig. S5). The DNA concentrations for the BGs and normal bacterial cells were 1.7 ± 1.5 and 78.5 ± 1.3 ng/μL, respectively (Table S2). These results indicated the genomic DNA in the as-prepared BGs had been substantially degraded.

Additionally, the fluorescence EEM analysis of the bulk solution of BGs in the absence and presence of TiO_2 nanoparticles shown that fluorescence intensity at 230/340 and 280/340 nm were insignificant and remained constant along with time (Fig. S3b). This implied that the as-prepared BGs had lost metabolic activity and no SMP was produced due to the evacuation of the cytoplasmic constituents, which would allow us to avoid the interferences induced by the presence of SMP in the nanoparticles-membrane interaction studies.

3.2 2D-FTIR-COS analysis on the interaction between TiO_2 nanoparticles and BGs.

The FTIR spectra of the BGs as a function of TiO_2 nanoparticle concentrations are shown in Fig. S6. The spectral variations mainly occurred in the 1700 − 1000 cm^{-1} region, where the absorption changed significantly. An increase in TiO_2 nanoparticles concentrations caused the characteristic bands changing to various degrees, indicating changes of vibrational structures in BGs by interacting with the TiO_2 nanoparticles. However, some of the bands strongly overlapped, and enhancement of the spectral resolution is needed to understand how individual IR band is subjected to the perturbation.

2D-FTIR-COS analysis can allow enhancing the spectral resolution by spreading overlap

peaks in a second dimension, and as a result simplifying the interpretation of one dimension spectrum. Fig. 3 illustrates the synchronous and asynchronous FTIR maps of BGs with TiO_2 nanoparticles as the perturbation. The FTIR regions of bacteria, corresponding to the wavelength ranges of 1000-1200, 1200-1400, and 1500-1700 cm^{-1}, could be roughly assigned to polysaccharide, phospholipid, and protein, respectively (Schmitt and Flemming, 1998). Detailed spectral assignments are presented in Table 1. In synchronous maps (Fig. 3b) most autopeaks, which locate on the diagonal, appear in the protein region, suggesting that protein mainly responses to concentration perturbation. A prominent peak at 1000 cm^{-1} was due to the increased TiO_2 concentration (Fig. S7) (Kiwi and Nadtochenko, 2005). Therefore, the cross peaks located at 1000 cm^{-1} in the synchronous and asynchronous map will not be taken into consideration. Closer observation of the protein region (Fig. 3a) shows that all the cross peaks, which locate off the diagonal, exhibit positive signs, indicating that theirs intensity change in the same direction.

The asynchronous map can provide information on the sequential order of specific structural response to perturbation based on the signs of the cross peaks. In this study, red color indicates a positive sign, while blue color indicates a negative sign in the asynchronous map (Figs. 3c and 3d). Likewise, most of the cross peaks of the asynchronous map located in protein region (Fig. 3d). Specifically, four characteristic cross peaks were observed at the bands of 1612-1674, 1565-1612, 1550-1565 and 1400-1500 cm^{-1} (Fig. 3c), and the four bands were assigned to C=O stretching, COO^- symmetric stretching, N-H (amide II) and aromatic C=C stretching, respectively.(Kiwi and Nadtochenko, 2005) The signs of the cross peaks (Table 1) indicate that sequential order of the bonding affinities of these bands with TiO_2 nanoparticles follow the order: COO^- → aromatic C=C stretching → N-H, amide II → C=O, ketone. It must be noted that the phospholipids and

polysaccharides might also contain functional groups such as COO^-, C=O and aromatic C=C. However, in terms of their abundance in bacteria, the protein are rich in these functionalities, while the characteristic functional moieties for polysaccharide and phospholipid are C-O and P=O, which did not response to the perturbation. Results herein could roughly imply that the protein play a major role in the binding process of cell membrane to the TiO_2 nanoparticles.

3.3 Settling experiments.

To further confirm the interpretation of the 2D-FTIR-COS results, a series of settling experiments were conducted using the selected protein, polysaccharide and lipid with TiO_2 nanoparticles. The settling curves of the test substances at concentrations ranging from 0 to 200 mg/L with TiO_2 were shown in Figs. 4a, b and c. Significant biomolecule-type-dependent settlings were observed. Only protein mixed with TiO_2 shows precipitation behavior at concentrations higher than 10 mg/L, suggesting that protein interact with TiO_2 much stronger than polysaccharide and phospholipid. The photos of settling experiments of the three test substances at concentration of 100 mg/L are provided in Fig. 5. Additionally, comparison of the A_{660} (absorbance at 660 nm) value of the test substances before and after mixed with TiO_2 were also calculated by the following equation:

$$\Delta A = A_{\mathrm{mixture}} - (A_{\mathrm{test\ substance}} + A_{\mathrm{TiO_2}}) \quad (4)$$

where A_{mixture} is the A_{660} of the mixture, and $A_{\mathrm{test\ substance}}$, $A_{\mathrm{TiO_2}}$ represent the individual A_{660} of the test substances and TiO_2. In principle, a positive ΔA indicates interaction between TiO_2 nanoparticles and test substances as a result of forming test substances-TiO_2 hetero-agglomeration

(Rieger *et al.*, 2004; Lin *et al.*, 2012). Conversely, zero or negative ΔA indicates no or very weak interaction between TiO_2 and the test substances. As shown in Fig. 4d, the ΔA had positive value at concentrations higher than 5 mg/L and exhibited an increasing trend with increasing concentrations, whereas no significant variations were observed with increasing polysaccharide and phospholipid concentrations mixed with TiO_2 nanoparticles. This suggests that TiO_2 nanoparticles preferentially interacted with protein and consequently formed larger hetero-agglomeration; while the interaction between TiO_2 nanoparticles and polysaccharide and phospholipid were weak or negligible.

4. Discussion

4.1 Increasing understanding of nanoparticle-cell membrane interaction.

Understanding the interaction between nanoparticle and cell membrane is a crucial step toward predicting subsequent biological effects (Hou *et al.*, 2012). As aforementioned, this interaction has been explored using various techniques and biological systems (e.g. cells and lipid bilayer) (Chen and Bothun, 2014). However, it is less clear what cell surface molecules are involved in the interaction (Chen and Bothun, 2014; Ma *et al.*, 2015). This work for the first time specifically investigated the nanoparticle-cell membrane interaction using BGs as a model cell membranes at molecular level with 2D-FTIR-COS technique. The results of this study, revealed by the 2D-FTIR-COS, demonstrated that cell membrane functionalities of protein preferentially interacted with TiO_2 nanoparticle; whereas the interaction of TiO_2 nanoparticle with C–OH (polysaccharide) and P=O (phospholipid) were very weak or insensitive to IR. Although this adds to the limited literature regarding the roles of bacterial cell envelope biomolecules in the nanoparticle-membrane

interaction, this finding is contradictory to previous reports. Jiang *et al.* (2010) previously reported that, in addition to protein, the lipopolysaccharide (LPS) also shown adhesive ability to metal oxides nanoparticles via hydrogen bonding with the O-antigen part (polysaccharide) using pure LPS extracted from *E. coli*. This discrepancy may have three possible explanations. First, the FTIR technique is insensitive to detect hydrogen bonding (Parikh and Chorover, 2006). Second, the level for LPS in *E. coli* K-12 bacterial cell envelope is much less than those for the phospholipid and protein, which are 4.73 and 4.83 times, respectively, higher than LPS level in terms molar ratio (Gmeiner and Schlecht, 1980). Third, the BGs maintain the phospholipid backbone structure with embedded protein, which may possibly compete with the LSP for absorption sites on the nanoparticles surfaces and thus leading to insignificant changes in the 2D-COS-FTIR response in the polysaccharide region. Whereas the study using extracted pure LPS only qualitatively represent the tendency of LPS to interact with nanoparticles regardless the three-dimensional structure of cell envelope. The current study cannot exclude the possibility of the interaction between LPS (polysaccharide) and TiO_2 nanoparticles when nanoparticles approach the bacterial surface. Nevertheless, our major findings herein indicate that protein plays dominant role in the interaction between TiO_2 nanoparticles and bacterial cell membrane. This was corroborated with the results from the settling experiments using standard protein, polysaccharide and phospholipid, which indicated the protein shown remarkable ability to form hetero-agglomeration with nanoparticles. Additionally, the asynchronous map of 2D-FTIR-COS indicates the propensities of functionalities bonded to TiO_2 nanoparticle followed as: COO^- > aromatic C=C stretching > N-H, amide II > C=O, ketone.

Knowledge on the interaction capacity and sequences of different biomolecules and functional

347 groups of cell membrane to nanoparticles is supposed to bring new insight into the
348 nanoparticle-membrane interactions and help to explain the toxicity of nanoparticles. For example,
349 the nano-toxicity may possibly depend on the adhesion of nanoparticles on the cell membrane
350 protein. Indeed, the cell membrane protein are suggested to be protected by the cell surface
351 polysaccharide polymers and thus unlikely to interact with large particles. The interaction between
352 the polysaccharide and large particle surface is unlikely to induce toxicity because this is similar to
353 the manner in which bacteria adhere to large surfaces through the surface polymers in natural
354 environment (Neu and Marshall, 1990). In contrast to their bulk counterparts, nanoparticles have
355 extremely small sizes and therefore very likely to be able to travel across the gap between the
356 surface polysaccharide polymers and reach the cell membrane surfaces. However, there exists
357 consensus that nanoparticles with high surface energy typically tend to aggregate to form
358 micro-scale agglomerates due to the unspecific interaction, thereby lowering their surface energy.
359 Thus the interaction behavior between nanoparticles and cell membrane has been frequently
360 elucidated as nanoparticles agglomerates with the cell membrane under static water condition and
361 underlying mechanism could be interpreted by the DLVO theory which considers the sum of
362 electrostatic and van der Waals interaction. This study conduct experiment under circumneutral
363 condition which is close to the IEP of TiO_2 nanoparticles and thus tend to aggregate according to
364 DLVO theory. In this case, there arises a concern that the results obtained from the micro-scale TiO_2
365 agglomerates did not realize the understanding in nano-scale. Nevertheless, it is important to note
366 that the DLVO theory were based on the assumption of steady-state behavior of agglomerates and
367 under static water conditions. We must recognize, however, that possible disruptions of aggregates
368 due to the force induced by water flows (i.e. friction and lubrication or shear force) should be

considered (Min *et al.*, 2008; Nel *et al.*, 2009). More importantly, natural and engineered aquatic systems typically under flowing condition. Therefore, the influence was environmental relevant and expected because of relative high agitation speed (200 rpm) were applied in this study. As a result, there should be likelihood of single nanoparticle or rafts from multiple particles directly bonding to the cell membrane surface protein due to their high propensity to interact with protein in the TiO_2-water-BGs system. This may lead to conformational changes of the protein and could be a possible reason for nanoparticle cytotoxicity. In this study, the changes in secondary structures of the protein in the BGs were characterized by the infrared self-deconvolution with second derivative resolution enhancement and with curve-fitting (Fig. S8). Results showed a decrease in α-helix contents and increase in the unordered and aggregate strands contents after exposed to nanoparticles (Table 2), indicating that the protein secondary structures were significantly changed and partial protein unfolding occurred after interacting with TiO_2 nanoparticles (Wu and Narsimhan, 2008). This is in accordance with the results of a previous study (Jiang *et al.*, 2010), which also suggested that the protein damaged when exposed to TiO_2 nanoparticles and as a consequence leading to loss physiological activities.

4.2 Significance for understanding the transport and fate of TiO_2 nanoparticles in natural system.

In fact, apart from NOM and bacteria, protein are ubiquitously present in aquatic environments, particularly in wastewater-impacted water, as a result from microbial metabolism or anthropogenic input (Hudson *et al.*, 2007; Meng *et al.*, 2013). TiO_2 nanoparticles is increasingly being used in commercial products and it will be inevitably released into aquatic environments. Therefore, TiO_2 will finally meet NOM, bacteria and protein, which are likely to influence their transport. A

391 previous study observed significant change in the aggregation state and deposition of TiO_2
392 nanoparticles in the presence of bacterial cells or/and NOM due to the changes of surface properties
393 (Chowdhury *et al.*, 2012). Nevertheless, how the protein affect the transport and fate of TiO_2
394 nanoparticles has seldom been considered. Our results herein suggested that the protein of the cell
395 envelope or in the bulk solution play a critical role in the interaction with TiO_2 nanoparticles. Thus,
396 the actual transport and fate of TiO_2 nanoparticles could be altered because the strong binding role
397 of protein, considering the ubiquitousness of soluble protein in aquatic systems, especially in the
398 anthropogenic-impact urban river with high SMP input from the waste water treatment plants
399 (WWTPs) effluent.

400 **4.3 Implications for the transport and fate of TiO_2 nanoparticles in engineered system.**

401 As the products of human activity, commercial TiO_2 nanoparticles have a high likelihood of
402 entering municipal sewage that flows to centralized WWTPs, in which biological treatments were
403 typically applied. It is very plausible that the majority of TiO_2 nanoparticles will be attached to the
404 cell surface proteins of the activated sludge (mainly microorganisms) therein and their fate will be
405 accompanied with the activated sludge. Given that the activated sludge could end up being as
406 agricultural land amendments (fertilizers), placed in landfills, incinerated, or dumped into oceans
407 (Kiser *et al.*, 2009), the subsequent ecological impact and relative risk assessment remain
408 unexplored and should be taken into consideration and examined in the future. In addition, the high
409 propensity of proteins or COO^--rich substances to interact with TiO_2 nanoparticles provides a
410 plausible clue for their removal in industrial wastewater where tremendous amount of TiO_2
411 nanoparticles waste are produced. Microorganisms/protein or COO^--rich substances could act as
412 coagulant to remove TiO_2 nanoparticles wastes by sequential treatments of coagulation, flocculation

and sedimentation (Serrao Sousa *et al.*, 2017).

4.4 Technological aspects

The elucidation of nanoparticle-membrane interaction is beneficial for the design of novel nanoparticles which can work effectively in the presence of bacteria in water and wastewater treatment. Furthermore, the nanoparticle properties (i.e. sizes and shapes) will also influence the nanoparticle-cell membrane interaction (Tong *et al.*, 2013b; Lin *et al.*, 2014); thus more types of TiO_2 nanoparticles with different sizes and morphologies (i.e. nanotubes, nanorods and nanosheet, etc.) should be examined in the future. On the other hand, variation in bacterial cell envelope structure profiles (i.e. lipids with different tail length or degree of saturation, the levels of outer membrane protein, and lipopolysaccharide, etc.) could be manipulated via genetic approaches using relative mutants (Gao *et al.*, 2012; Huang *et al.*, 2015). BGs derived from the cell envelope-related mutants will enable one to determine the role of the interested gene products in the interaction between cell membrane and nanoparticles. Additionally, as membrane construction of Gram-positive and the Gram-negative bacteria are different, further studies using the BGs derived from Gram-positive bacteria (Abrams and Mcnamara, 1962) are therefore warranted. In general, the approach using BGs as model cell membrane combined with the 2D-FTIR-COS technique would provide an ideal platform to reveal the bionano surface interaction mechanism at molecular level.

5. Conclusions

The interaction between TiO_2 nanoparticles and bacterial cell membrane was investigated at molecular level using 2D-FTIR-COS analysis and BGs as model cell envelope. The main

conclusions are:

- The synchronous map of 2D-FTIR-COS results shown that the functionalities in proteins of BGs have high propensity to interacted with TiO_2 nanoparticles, whereas the interaction of TiO2 nanoparticles with polysaccharides (C–OH) and phospholipids (P=O) were not detected under the test condition.
- The asynchronous map of 2D-FTIR-COS suggested a sequential order of functionalities bonded to TiO_2 nanoparticles with the order from high to low: COO^- > aromatic C=C stretching > N-H, amide II > C=O, ketone. These findings highlighted the role of protein in the interaction mechanisms between nanoparticles and bacterial cell membrane.
- Co-settling of TiO_2 nanoparticles with pure biomolecules (i.e., protein, polysaccharide and phospholipid) also highlighted the high propensity of protein molecules to interact with TiO_2 nanoparticles.
- 2D-FTIR-COS analysis using BGs as model cell membrane were shown to be a promising approach to investigating the molecular mechanisms by which nanoparticles interacting with bacterial cell membrane.
- This study could enhance our current knowledge on interaction mechanism of TiO_2 nanoparticles with bacterial cell membrane in water and has important implication for the nanotoxicity as well as the transport and fate of TiO_2 nanoparticles in the natural and engineered systems.

Associated content

Supporting Information

Additional detail information including protocols for light microscopy observation, scanning electronic microscopy (SEM), transmission electron microscopy (TEM), atomic force microscopy (AFM), X-ray diffraction patterns (XRD) and curve-fitted FTIR spectra; and Tables showing the minimum inhibition concentration and maximum growth concentration for *E. coli* K-12 (Table S1), and DNA contents of BGs and normal bacterial cells (Table S2); and Figures showing the XRD pattern (Fig. S1) and TEM image (Fig. S2) of Degussa P25TiO_2 nanoparticles, fluorescence intensity evolution (Fig. S3), light microscopy images (Fig. S4), Agarose gel electrophoresis results (Fig. S5), FTIR spectra of BGs with TiO_2 nanoparticles (Fig. S6) and TiO_2 nanoparticles alone (Fig. S7), second derivative resolution enhanced and curve-fitted amide I region for protein secondary structure of BGs (Fig. S8).

Acknowledgments

The project was supported by a research grant (GRF14100115) of the Research Grant Council, Hong Kong SAR Government. The project was also support by a Direct Grant from the Research Committee and a Technology and Business Development Fund (TBF15SCI008) from the Office of Research and Knowledge Transfer Services of The Chinese University of Hong Kong, and the research grant (41573086 and 41425015) of National Science Foundation of China to G.Y. Li and T.C. An. P.K. Wong was also supported by CAS/SAFEA International Partnership Program for Creative Research Teams.

477 **Figure Captions**

478 **Fig. 1** Fluorescence contour plots of the SMP secreted by (a) *E. coli* cells under dark; (b) *E. coli*
479 K-12 under dark with the presence of TiO_2 nanoparticles (100 mg/L).

480 **Fig. 2** SEM and AFM images of the normal *E. coli* K-12 cell (a, c) and bacterial ghost (b, d),
481 respectively.

482 **Fig. 3** Synchronous (a, b) and asynchronous (c, d) 2D-FTIR-COS maps generated from the
483 1700-1300 cm^{-1} region (a, c) and 1700-1000 cm^{-1} region (b, d) of the FTIR spectra of BGs
484 with the increasing TiO_2 nanoparticles concentrations.

485 **Fig. 4** (a) Settling curves of standard protein, (b) polysaccharide, (c) phospholipid with 100
486 mg/TiO_2 nanoparticles; and (d) the difference of absorbance at 660 nm of the test substances
487 before and after mixed with TiO_2 nanoparticles.

488 **Fig. 5** Photos of the settling experiments of test substances with TiO2 nanoparticle.

489

References

Abrams, A. and Mcnamara, P., 1962. Polynucleotide phosphorylase in isolated bacterial cell membranes. *Journal of Biological Chemistry* 237(1), 170-175.

Amara, A.A., Salem-Bekhit, M.M. and Alanazi, F.K., 2013a. Preparation of bacterial ghosts for *E. coli* JM109 using sponge-like reduced protocol. *Asian Journal of Biological Sciences* 6, 363-369.

Amara, A.A., Salem-Bekhit, M.M. and Alanazi, F.K., 2013b. Sponge-like: A new protocol for preparing bacterial ghosts. *Scientific World Journal* 2013, 545741.

Andrews, J.M., 2001. Determination of minimum inhibitory concentrations. *Journal of Antimicrobial Chemotherapy* 48, 5-16.

Auffan, M., Pedeutour, M., Rose, J., Masion, A., Ziarelli, F., Borschneck, D., Chaneac, C., Botta, C., Chaurand, P., Labille, J. and Bottero, J.Y., 2010. Structural degradation at the surface of a TiO_2-based nanomaterial used in cosmetics. *Environmental Science & Technology* 44(7), 2689-2694.

Chen, K.L. and Bothun, G.D., 2014. Nanoparticles meet cell membranes: probing nonspecific interactions using model membranes. *Environmental Science & Technology* 48(2), 873-880.

Chen, W., Habibul, N., Liu, X.Y., Sheng, G.P. and Yu, H.Q., 2015. FTIR and synchronous fluorescence heterospectral two-dimensional correlation analyses on the binding characteristics of copper onto dissolved organic matter. *Environmental Science & Technology* 49(4), 2052-2058.

Chen, W., Qian, C., Liu, X.Y. and Yu, H.Q., 2014. Two-dimensional correlation spectroscopic analysis on the interaction between humic acids and TiO_2 nanoparticles. *Environmental*

512 *Science & Technology* 48(19), 11119-11126.

513 Chowdhury, I., Hong, Y., Honda, R.J. and Walker, S.L., 2011. Mechanisms of TiO_2 nanoparticle
514 transport in porous media: Role of solution chemistry, nanoparticle concentration, and flow
515 rate. *Journal of Colloid and Interface Science* 360(2), 548-555.

516 Chowdhury, I., Cwiertny, D.M. and Walker, S.L., 2012. Combined factors influencing the
517 aggregation and deposition of nano-TiO_2 in the presence of humic acid and bacteria.
518 *Environmental Science & Technology* 46(13), 6968-6976.

519 Dluhy, R., Shanmukh, S. and Morita, S.I., 2006. The application of two-dimensional correlation
520 spectroscopy to surface and interfacial analysis. *Surface and Interface Analysis* 38(11),
521 1481-1496.

522 French, R.A., Jacobson, A.R., Kim, B., Isley, S.L., Penn, R.L. and Baveye, P.C., 2009. Influence of
523 ionic strength, pH, and cation valence on aggregation kinetics of titanium dioxide
524 nanoparticles. *Environmental Science & Technology* 43(5), 1354-1359.

525 Gao, M., An, T., Li, G., Nie, X., Yip, H.Y., Zhao, H. and Wong, P.K., 2012. Genetic studies of the
526 role of fatty acid and coenzyme A in photocatalytic inactivation of Escherichia coli. *Water*
527 *Research* 46(13), 3951-3957.

528 Gmeiner, J. and Schlecht, S., 1980. Molecular composition of the outer-membrane of *Escherichia*
529 *coli* and the importance of protein-lipopolysaccharide interactions. *Archives Of Microbiology*
530 127(2), 81-86.

531 Hoffmann, M.R., Martin, S.T., Choi, W.Y. and Bahnemann, D.W., 1995. Environmental applications
532 of semiconductor photocatalysis. *Chemical Reviews* 95(1), 69-96.

533 Hou, W.C., Moghadam, B.Y., Corredor, C., Westerhoff, P. and Posner, J.D., 2012. Distribution of

functionalized gold nanoparticles between water and lipid bilayers as model cell membranes. *Environmental Science & Technology* 46(3), 1869-1876.

Huang, G.C., Xia, D.H., An, T.C., Ng, T.W., Yip, H.Y., Li, G.Y., Zhao, H.J. and Wong, P.K., 2015. Dual roles of capsular extracellular polymeric substances in photocatalytic inactivation of *Escherichia coli*: comparison of *E. coli* BW25113 and isogenic mutants. *Applied and Environmental Microbiology* 81(15), 5174-5183.

Hudson, N., Baker, A. and Reynolds, D., 2007. Fluorescence analysis of dissolved organic matter in natural, waste and polluted waters - A review. *River Research and Applications* 23(6), 631-649.

Jalava, K., Hensel, A., Szostak, M., Resch, S. and Lubitz, W., 2002. Bacterial ghosts as vaccine candidates for veterinary applications. *Journal of Controlled Release* 85(1-3), 17-25.

Jiang, W., Yang, K., Vachet, R.W. and Xing, B.S., 2010. Interaction between oxide nanoparticles and biomolecules of the bacterial cell envelope as examined by infrared spectroscopy. *Langmuir* 26(23), 18071-18077.

Keller, C.A. and Kasemo, B., 1998. Surface specific kinetics of lipid vesicle adsorption measured with a quartz crystal microbalance. *Biophysical Journal* 75(3), 1397-1402.

Khan, S.S., Srivatsan, P., Vaishnavi, N., Mukherjee, A. and Chandrasekaran, N., 2011. Interaction of silver nanoparticles (SNPs) with bacterial extracellular proteins (ECPs) and its adsorption isotherms and kinetics. *Journal of hazardous materials* 192(1), 299-306.

Kiser, M.A., Westerhoff, P., Benn, T., Wang, Y., Perez-Rivera, J. and Hristovski, K., 2009. Titanium nanomaterial removal and release from wastewater treatment plants. *Environmental Science & Technology* 43(17), 6757-6763.

Kiwi, J. and Nadtochenko, V., 2005. Evidence for the mechanism of photocatalytic degradation of

556 the bacterial wall membrane at the TiO_2 interface by ATR-FTIR and laser kinetic spectroscopy.
557 *Langmuir* 21(10), 4631-4641.

558 Kudela, P., Koller, V.J. and Lubitz, W., 2010. Bacterial ghosts (BGs)-Advanced antigen and drug
559 delivery system. *Vaccine* 28(36), 5760-5767.

560 Leroueil, P.R., Hong, S.Y., Mecke, A., Baker, J.R., Orr, B.G. and Holl, M.M.B., 2007. Nanoparticle
561 interaction with biological membranes: Does nanotechnology present a janus face? *Accounts of*
562 *chemical research* 40(5), 335-342.

563 Lesniak, A., Salvati, A., Santos-Martinez, M.J., Radomski, M.W., Dawson, K.A. and Aberg, C.,
564 2013. Nanoparticle adhesion to the cell membrane and its effect on nanoparticle uptake
565 efficiency. *Journal of the American Chemical Society* 135(4), 1438-1444.

566 Li, K.G., Zhang, W., Huang, Y. and Chen, Y.S., 2011. Aggregation kinetics of CeO_2 nanoparticles in
567 KCl and $CaCl_2$ solutions: measurements and modeling. *Journal of Nanoparticle Research*
568 13(12), 6483-6491.

569 Lin, D.H., Ji, J., Long, Z.F., Yang, K. and Wu, F.C., 2012. The influence of dissolved and
570 surface-bound humic acid on the toxicity of TiO_2 nanoparticles to *Chlorella* sp. *Water Research*
571 46(14), 4477-4487.

572 Lin, X.C., Li, J.Y., Ma, S., Liu, G.S., Yang, K., Tong, M.P. and Lin, D.H., 2014. Toxicity of TiO_2
573 nanoparticles to *Escherichia coli*: Effects of particle size, crystal phase and water chemistry.
574 *PLoS One* 9(10).

575 Ma, S., Zhou, K.J., Yang, K. and Lin, D.H., 2015. Heteroagglomeration of oxide nanoparticles with
576 algal cells: effects of particle type, ionic strength and pH. *Environmental Science &*
577 *Technology* 49(2), 932-939.

578 Mahon, E., Salvati, A., Bombelli, F.B., Lynch, I. and Dawson, K.A., 2012. Designing the
579 nanoparticle-biomolecule interface for "targeting and therapeutic delivery". *Journal of*
580 *Controlled Release* 161(2), 164-174.
581 Mayr, U.B., Walcher, P., Azimpour, C., Riedmann, E., Haller, C. and Lubitz, W., 2005. Bacterial
582 ghosts as antigen delivery vehicles. *Advanced Drug Delivery Reviews* 57(9), 1381-1391.
583 Mecozzi, M., Pietrantonio, E. and Pietroletti, M., 2009. The roles of carbohydrates, proteins and
584 lipids in the process of aggregation of natural marine organic matter investigated by means of
585 2D correlation spectroscopy applied to infrared spectra. *Spectrochimica Acta Part A-Molecular*
586 *and Biomolecular Spectroscopy* 71(5), 1877-1884.
587 Menard, A., Drobne, D. and Jemec, A., 2011. Ecotoxicity of nanosized TiO_2. Review of in vivo data.
588 *Environmental Pollution* 159(3), 677-684.
589 Meng, F.G., Huang, G.C., Yang, X., Li, Z.Q., Li, J., Cao, J., Wang, Z.G. and Sun, L., 2013.
590 Identifying the sources and fate of anthropogenically impacted dissolved organic matter (DOM)
591 in urbanized rivers. *Water Research* 47(14), 5027-5039.
592 Min, Y.J., Akbulut, M., Kristiansen, K., Golan, Y. and Israelachvili, J., 2008. The role of
593 interparticle and external forces in nanoparticle assembly. *Nature Materials* 7(7), 527-538.
594 Mukherjee, B. and Weaver, J.W., 2010. Aggregation and charge behavior of metallic and
595 nonmetallic nanoparticles in the presence of competing similarly-charged inorganic ions.
596 *Environmental Science & Technology* 44(9), 3332-3338.
597 Nel, A.E., Madler, L., Velegol, D., Xia, T., Hoek, E.M.V., Somasundaran, P., Klaessig, F.,
598 Castranova, V. and Thompson, M., 2009. Understanding biophysicochemical interactions at
599 the nano-bio interface. *Nature Materials* 8(7), 543-557.

600 Neu, T.R. and Marshall, K.C., 1990. Bacterial polymers: physicochemical aspects of their
601 interactions at interfaces. *Journal Of Biomaterials Applications* 5(2), 107-133.
602 Ni, B.J., Rittmann, B.E. and Yu, H.Q., 2011. Soluble microbial products and their implications in
603 mixed culture biotechnology. *Trends in Biotechnology* 29(9), 454-463.
604 Noda, I., 1993. Generalized two-dimensional correlation method applicable to infrared, Raman, and
605 other types of spectroscopy. *Applied Spectroscopy* 47(9), 1329-1336.
606 Nohynek, G.J., Lademann, J., Ribaud, C. and Roberts, M.S., 2007. Grey goo on the skin?
607 Nanotechnology, cosmetic and sunscreen safety. *Critical Reviews In Toxicology* 37(3),
608 251-277.
609 Parikh, S.J. and Chorover, J., 2006. ATR-FTIR spectroscopy reveals bond formation during
610 bacterial adhesion to iron oxide. *Langmuir* 22(20), 8492-8500.
611 Rieger, L., Langergraber, G., Thomann, M., Fleischmann, N. and Siegrist, H., 2004. Spectral in-situ
612 analysis of NO_2, NO_3, COD, DOC and TSS in the effluent of a WWTP. *Water Science and*
613 *Technology* 50(11), 143-152.
614 Roiter, Y., Ornatska, M., Rammohan, A.R., Balakrishnan, J., Heine, D.R. and Minko, S., 2008.
615 Interaction of nanoparticles with lipid membrane. *Nano Letters* 8(3), 941-944.
616 Rusciano, G., De Luca, A.C., Pesce, G. and Sasso, A., 2009. On the interaction of nano-sized
617 organic carbon particles with model lipid membranes. *Carbon* 47(13), 2950-2957.
618 Saptarshi, S.R., Duschl, A. and Lopata, A.L., 2013. Interaction of nanoparticles with proteins:
619 relation to bio-reactivity of the nanoparticle. *Journal of Nanobiotechnology* 11.
620 Schmitt, J. and Flemming, H.C., 1998. FTIR-spectroscopy in microbial and material analysis.
621 *International Biodeterioration & Biodegradation* 41(1), 1-11.

622 Schwegmann, H., Ruppert, J. and Frimmel, F.H., 2013. Influence of the pH-value on the
623 photocatalytic disinfection of bacteria with TiO_2 - Explanation by DLVO and XDLVO theory.
624 *Water Research* 47(4), 1503-1511.
625 Serrao Sousa, V., Corniciuc, C. and Ribau Teixeira, M., 2017. The effect of TiO_2 nanoparticles
626 removal on drinking water quality produced by conventional treatment C/F/S. *Water Research*
627 109, 1-12.
628 Shih, Y.H., Zhuang, C.M., Peng, Y.H., Lin, C.H. and Tseng, Y.M., 2012. The effect of inorganic ions
629 on the aggregation kinetics of lab-made TiO_2 nanoparticles in water. *Science of the Total*
630 *Environment* 435, 446-452.
631 Tong, T.Z., Binh, C.T.T., Kelly, J.J., Gaillard, J.F. and Gray, K.A., 2013a. Cytotoxicity of
632 commercial nano-TiO_2 to *Escherichia coli* assessed by high-throughput screening: Effects of
633 environmental factors. *Water Research* 47(7), 2352-2362.
634 Tong, T.Z., Shereef, A., Wu, J.S., Binh, C.T.T., Kelly, J.J., Gaillard, J.F. and Gray, K.A., 2013b.
635 Effects of material morphology on the phototoxicity of nano-TiO_2 to bacteria. *Environmental*
636 *Science & Technology* 47(21), 12486-12495.
637 Wang, L.P., Shen, Q.R., Yu, G.H., Ran, W. and Xu, Y.C., 2012. Fate of biopolymers during rapeseed
638 meal and wheat bran composting as studied by two-dimensional correlation spectroscopy in
639 combination with multiple fluorescence labeling techniques. *Bioresource Technology* 105,
640 88-94.
641 Weir, A., Westerhoff, P., Fabricius, L., Hristovski, K. and von Goetz, N., 2012. Titanium dioxide
642 nanoparticles in food and personal care products. *Environmental Science & Technology* 46(4),
643 2242-2250.

644 Wu, X. and Narsimhan, G., 2008. Characterization of secondary and tertiary conformational
645 changes of beta-lactoglobulin adsorbed on silica nanoparticle surfaces. *Langmuir* 24(9),
646 4989-4998.

647 Zhang, X.F. and Yang, S.H., 2011. Nonspecific adsorption of charged quantum dots on supported
648 zwitterionic lipid bilayers: Real-time monitoring by quartz crystal microbalance with
649 dissipation. *Langmuir* 27(6), 2528-2535.

Table 1. 2D-FTIR-COS result on the assignment and sign of each cross-peak in synchronous and asynchronous (in the brackets) map of BGs with increasing TiO_2 nanoparticle concentrations (Signs were obtained in the upper-left corner of the maps).

Region	Position (cm^{-1})	Possible assignment	Sign					
			Protein				Phosphate	Polysaccharide
			1612 - 1674	1565 - 1612	1550 - 1565	1400 - 1500	1200 - 1250	1100 - 1170
Protein	1612 - 1674	amide I, C=O stretching	+	+ (-)	+ (+)	+ (-)	+ (+)	+ (+)
	1565 - 1612	aspartate or glutamate COO^- symmetric stretching		+	+ (+)	+ (+)	+ (+)	+ (+)
	1550 - 1565	amide II, N-H, C-N of protein			+	+ (-)	+ (+)	+ (+)
	1400 - 1500	aromatic C=C stretching, C-H bend from CH_2				+	+ (+)	+ (+)
Phosphate	1200 - 1250	P=O from phosphate					0	+ (0)
Polysaccharide	1100 - 1170	C-O stretching of polysaccharide						0

Table 2. Band assignments for protein secondary structures of BGs and changes of the protein secondary structures exposed to increasing TiO_2 nanoparticles concentrations estimated by the curve fitting of the amide I region (1600 -1700 cm^{-1}) from the FT-IR spectra.

Secondary structures	Wavenumber (cm^{-1})	TiO_2 concentrations (mg/L)					
		0	25	50	100	150	200
Aggregated strands	1625-1610	5.25 %	12.48 %	12.36 %	16.48 %	16.60 %	21.60 %
β-Sheet	1640-1630	28.31 %	24.53 %	25.44 %	30.72 %	28.30 %	19.79 %
Unordered	1645-1640	-	14.99 %	15.11 %	15.34 %	15.86 %	19.50 %
α-Helix	1657-1648	35.71 %	17.61 %	18.41 %	15.65 %	16.53 %	18.11 %
3-Turn helix	1666-1659	22.41 %	19.36 %	18.82 %	15.00 %	15.96 %	16.56 %
Antiparallel β-sheet/aggregated strands	1695-1680	8.32 %	10.95 %	9.82 %	6.78 %	6.72 %	4.40 %

Fig. 1

(a) *E. coli* K-12 under dark

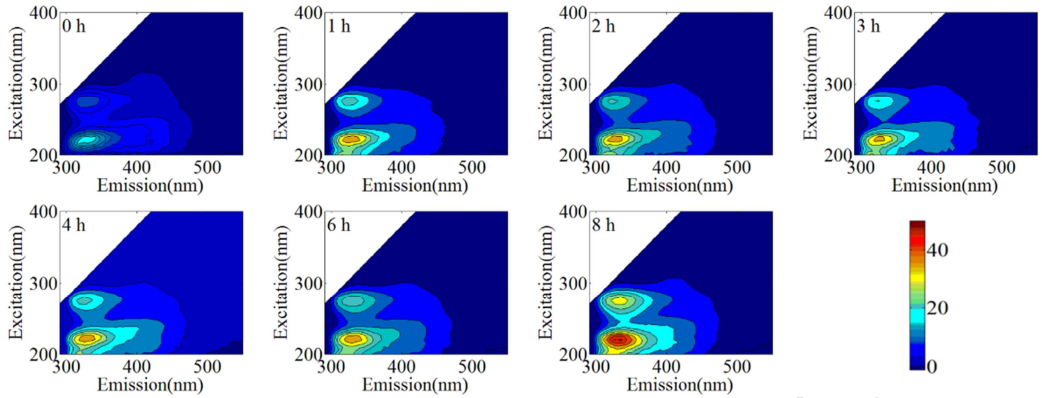

(b) *E. coli* K-12 under dark with TiO_2 nanoparticles

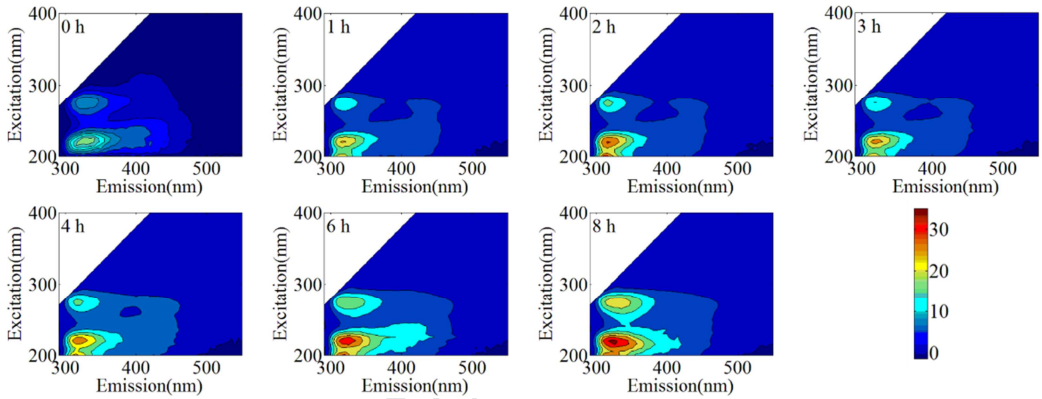

Fig. 2

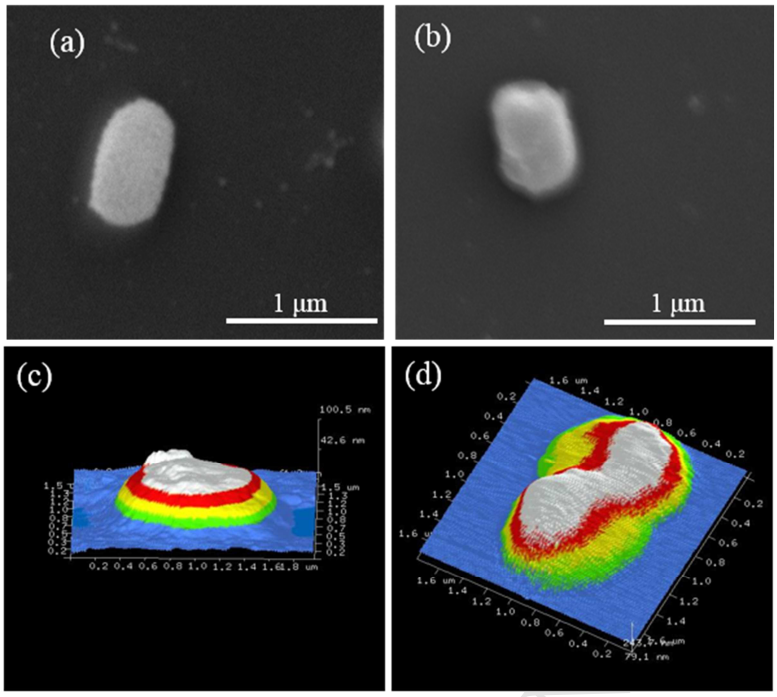

Fig. 3

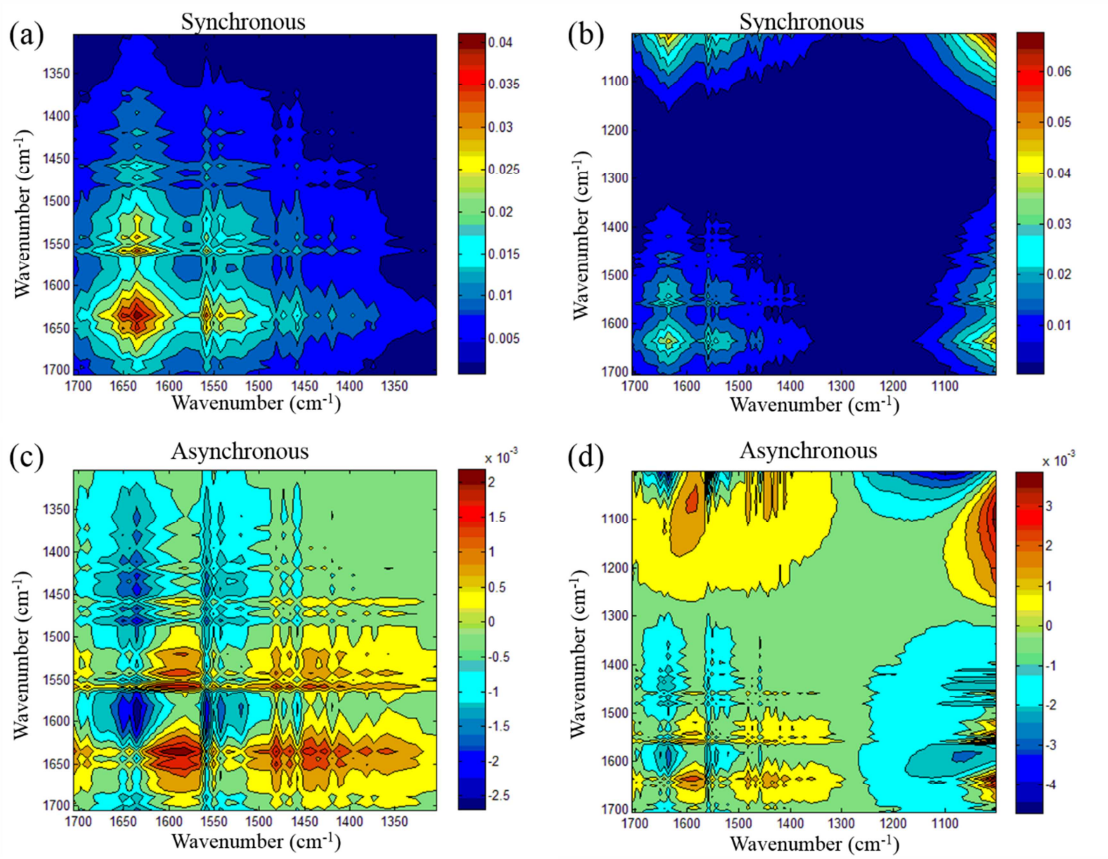

Fig. 4

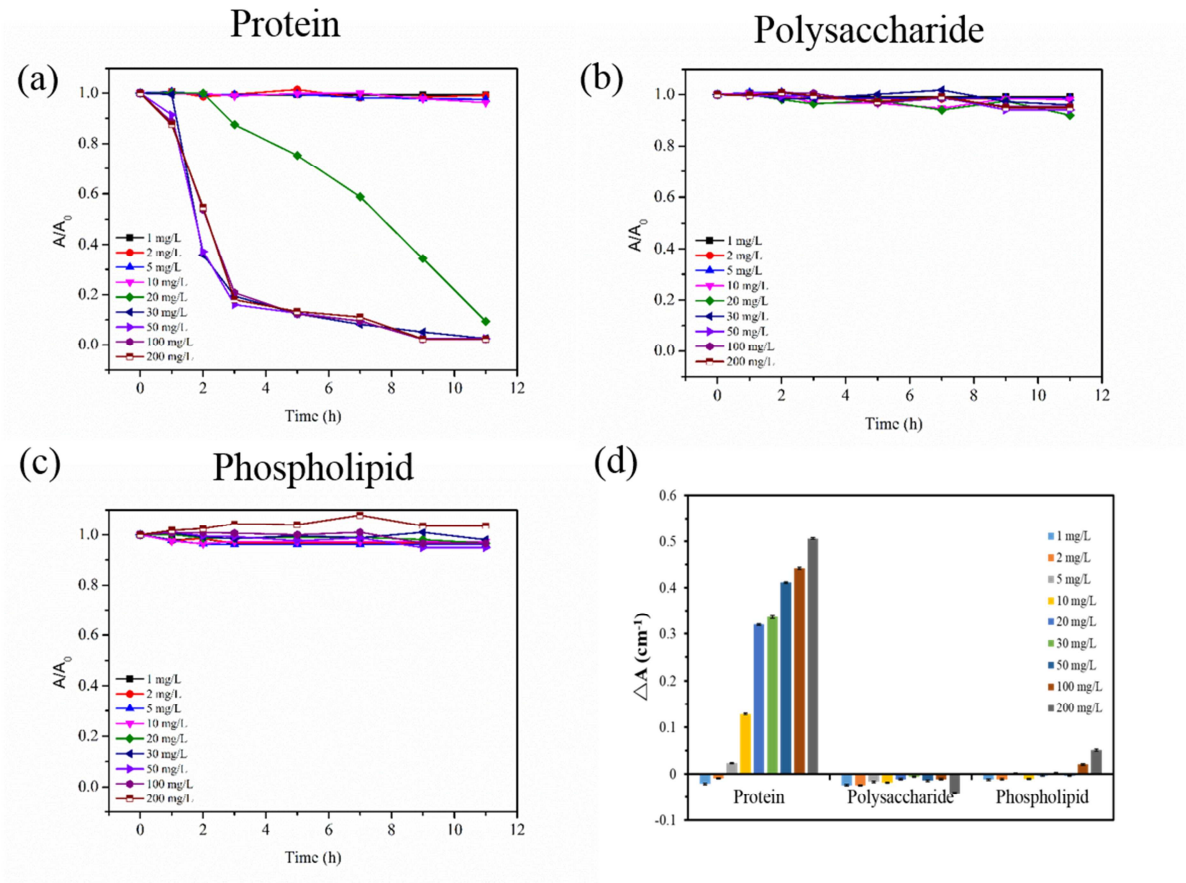

Fig. 5

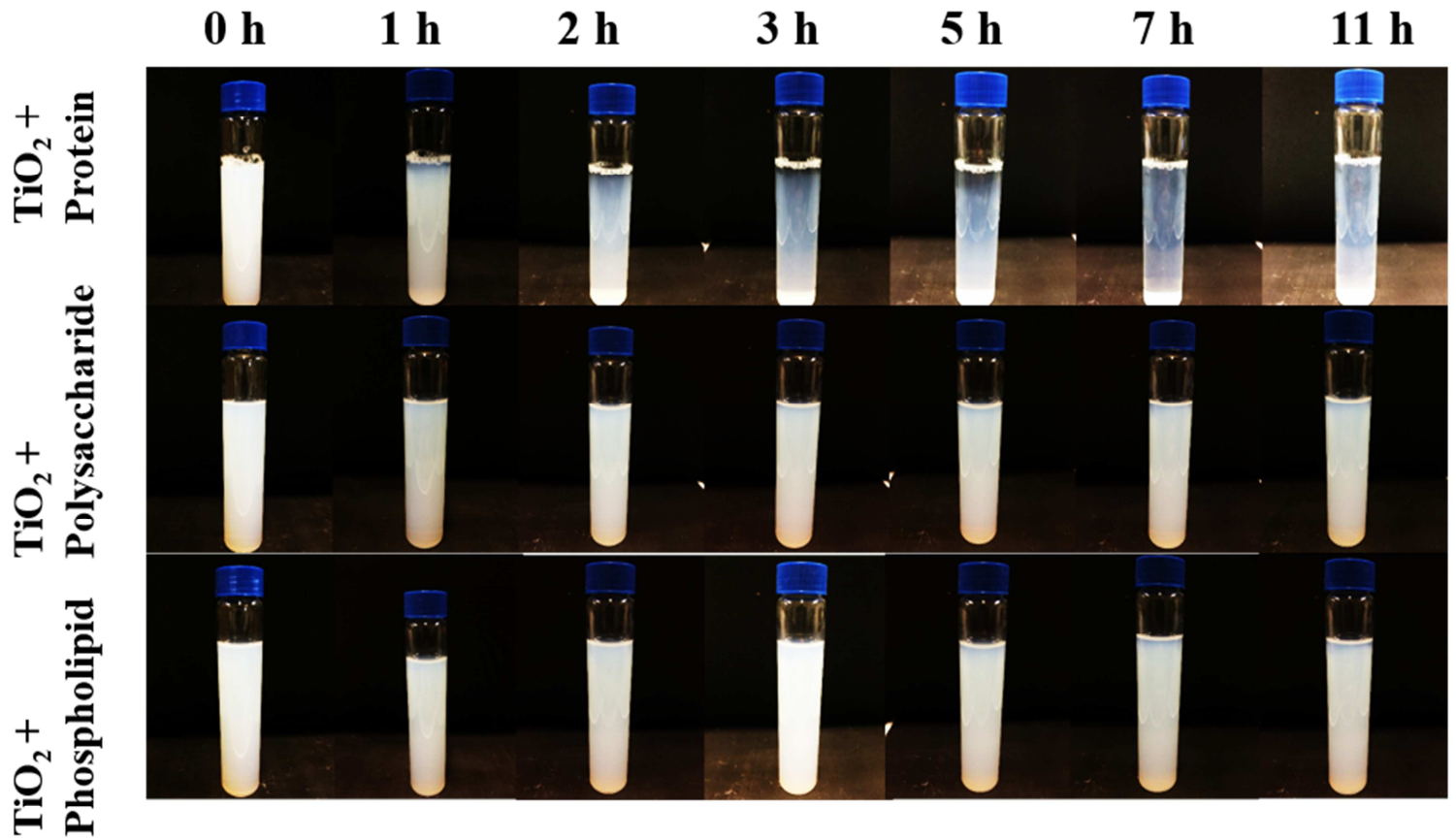
0 h
1 h
2 h
3 h
5 h
7 h
11 h
TiO2 + Protein
TiO2 + Polysaccharide
TiO2 + Phospholipid

Highlights

- Interaction between bacterial cell membranes and nano-TiO_2 were studied at molecular level.
- Bacterial ghosts devoid of cytoplasm were used as model cell membrane.
- 2D-COS results suggested a sequential order of functionalities bonded to nano-TiO_2.
- Protein played the most important role in the interaction mechanism.